Dalton Transactions

RSC Publishing

PAPER

View Article Online
View Journal | View Issue

Cite this: *Dalton Trans.*, 2013, **42**, 14826

Co-ordinative properties of a tripodal trisamide ligand with a capped octahedral preference†

Fawaz A. Saad,[a,b] James C. Knight,[a] Benson M. Kariuki[a] and Angelo J. Amoroso*[a]

Received 4th July 2013,
Accepted 31st July 2013

DOI: 10.1039/c3dt51791h

www.rsc.org/dalton

An investigation into the co-ordination chemistry of tris(6-pivaloylamino-2-pyridylmethyl)amine (TPPA) shows a preference for capped octahedral geometry when no additional donors are present. This tripodal ligand yields capped octahedral complexes upon co-ordination to a series of first row transition metals when the counter-ion is a perchlorate, bromide or iodide ion. The exact geometry has been confirmed by shape mapping calculations. The largest variation from the capped octahedral geometry is observed in the case of nickel(II), indicating a greater octahedral preference of this metal ion.

Introduction

The tripodal tetraamine ligand, tris(2-pyridylmethyl)amine (TPA), was first synthesised in 1967 by Anderegg and Wenk,[1] and its co-ordination chemistry has since been extensively studied.[2–6] The TPA framework (Fig. 1) is sterically suited to co-ordinating *via* a trigonal pyramidal arrangement of donor atoms, and typically an additional ligand will approach axially to give a trigonal bipyramidal co-ordination geometry around the metal cation. Although there are several exceptions to this, such as the co-ordination to Pt(II) and Pd(II), which prefer square planar geometries, causing the ligand to bind in a hypodentate manner in which one pyridine does not co-ordinate.[7,8] Similar tridentate co-ordination modes have also been observed upon co-ordination to ruthenium(II)[9] and iron(II).[10]

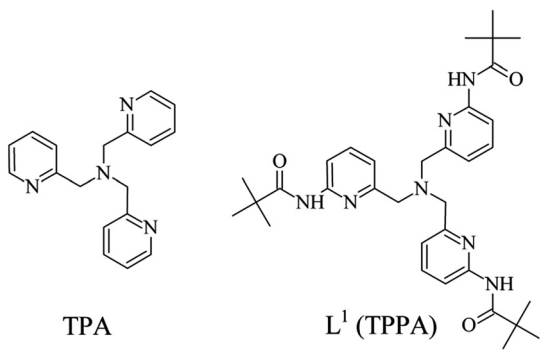

Fig. 1 The ligand under investigation, L^1 (right), alongside TPA (left).

While seven- and eight-coordinate complexes of TPA have been reported, for example, $[Fe(TPA)_2](BPh_4)_2$ [10] and $[Mn(TPA)_2](ClO_4)_2$ [11] (each contains two tetradentate TPA groups per metal ion), it is interesting that derivatives of TPA (such as TPPA), where the pyridyl groups are substituted with additional donor atoms,[5,12,13] generally result in the isolation of five co-ordinate species even though they are potentially heptadentate. Presumably, this is due to poor metal–ligand interactions in this geometry meaning that the five co-ordinate geometry is favourable. However, the nature of these substituents and the position on the pyridyl rings have been shown to have significant effects on the structural and physical properties of their metal complexes.[14–16]

A common set of derivatives of TPA is generated by alkyl substitution at the 6-position of the pyridyl groups. This simple modification can produce unfavourable steric interactions which influence the ligand's ability to bind to the metal. In a few reported examples of TPA, substituents at the 6-position on each of the pyridyl groups have been shown to block further co-ordination entirely; for example, some TPA derivatives containing methyl[15,16] and phenyl[17] functionalities have been reported which, upon complexation to Cu(I) cations, lead to four-coordinate Cu(I) complexes.

Mareque Rivas[18] and others[19] have carried out investigations into the hydrogen bond donor properties of complexes of tris(2-pyridylmethyl)amine (TPA) derivatives, with respect to their ability to interact with the auxiliary ligand occupying the final axial co-ordination site of the complex. Despite the heptadentate nature of this ligand, only five co-ordinate complexes have been reported to date. This may be due to the nature of the mixture of ligands available to the metal centre. With this in mind, we set out to determine whether, in the absence of other suitable ligands, seven co-ordinate species could be isolated from TPPA. In addition, as only Cu(II) complexes of TPPA have been crystallographically characterised, we investigated

[a]*School of Chemistry, Cardiff University, Cardiff, UK. E-mail: amorosoaj@cf.ac.uk*
[b]*Umm Al-Qura University, Kingdom of Saudi Arabia*

†CCDC 948550–948556. For crystallographic data in CIF or other electronic format see DOI: 10.1039/c3dt51791h

the co-ordination of this ligand with other transition metal ions.

Experimental

All reagents and solvents were purchased from commercial sources and used as received, unless noted otherwise. NMR spectra were measured using a Bruker AM 250–400 or Bruker Av-500 Plus FT-NMR spectrometer. Residual signals of the solvent were used for reference for ^{1}H and ^{13}C NMR. For infrared spectra, each compound was pressed into a disk with an excess of dried KBr and measured using a Jasco 660 FT-IR spectrophotometer. Electrospray (ES) and high-resolution (HR) mass spectra were measured using a Waters LCT Premier XE (oa-TOF) mass spectrometer. UV-vis absorption spectra were run in HPLC grade acetonitrile (Fisher) and measured using a Jasco V-570 spectrophotometer from 230 to 1100 nm (optical path length 1.0 cm). Elemental analyses were carried out by the Warwick Analytical Service, University of Warwick.

The cyclic voltammetry experiments were carried out using an AUTOLAB PGSTAT12 potentiostat in conjunction with the General Purpose Electrochemical System software (GPES version 4.7 for Windows) in a specially designed three-electrode glass cell with a Teflon-coated cell cap. A bioanalytical platinum working electrode (model no. MF2013) with a 1.6 mm disk was used for all experiments. The counter electrode was a platinum wire and the reference electrode an $Ag/AgNO_3$ electrode. To regain electrochemical sensitivity and reproducibility the working electrode was polished, with 600 grid emery paper, to a mirror surface and then ultrasonicated. Prior to each experiment, the electrode was washed with high performance liquid chromatography (HPLC) grade CH_3CN and dried in air for about 15 min. A 0.1 M $[Bu_4N][PF_6]$ solution in CH_3CN was used as the supporting electrolyte. In all cases, ferrocene was used as an internal reference. Solutions were degassed with nitrogen and a nitrogen atmosphere was maintained over the solution during the experiment.

Trisamide (TPPA) L^1

Tris(6-pivaloylamino-2-pyridylmethyl)amine (TPPA) was prepared as reported by Harata *et al.*[20]

^{1}H-NMR δ_H (250 MHz; $CDCl_3$): 1.25 (27H, s); 3.69 (6H, s); 7.20 (3H, d, Ar, J = 7.4 Hz); 7.60 (3H, t, Ar, J = 7.8 Hz); 7.94 (3H, s, NH); 8.04 (3H, d, Ar, J = 8.1 Hz); ^{13}C δ_C (62.5 MHz; $CDCl_3$): 27.4, 39.7, 59.6, 112.1, 118.5, 138.8, 138.8, 150.9, 177.0; accurate ESMS (m/z): 610.3505 (100), $[L + Na]^+$ [calculated 610.3481], 588.3676 (80) $[L + H]^+$ [calculated 588.3676]; IR KBr/cm^{-1}: ν = 3429m, 1691s; UV/Vis [λ_{max}, nm (εM, M^{-1} cm^{-1})] in CH_3CN: 320.5 (1811), 284.5 (17 915), 243.5 (21 865).

General procedure for the synthesis of metal complexes

The ligand (1 equivalent, typically 0.085 mmol) was dissolved in the minimum amount of acetonitrile (typically 3 mL). The solutions were warmed to *ca.* 60 °C to ensure that the ligand fully dissolved. To this stirring solution, the metal perchlorate, chloride or iodide salt (1 equivalent) dissolved in acetonitrile (typically ~2 mL) was added dropwise. Recrystallisation of the compounds typically involved the diffusion of diethyl ether into acetonitrile solutions which were filtered through Celite. The yields from these reactions were moderate to high (25–97%). This crystalline material was then subsequently used for all spectroscopic measurements.

WARNING: Perchlorate salts of metal complexes are potentially explosive. Care should be taken while handling such complexes.

$[MnC_{33}H_{45}N_7O_3]\cdot[ClO_4][Br]\cdot CH_3CN$ (1). Cream-coloured plate crystals (46% yield); accurate ESMS (m/z): 641.2864 (10) $[Mn(L^1) - H]^+$ [calculated 641.2886]; $MnC_{35}H_{48}N_8O_3BrClO_4$ (found: C, 48.84; H, 5.72; N, 13.21% requires C, 48.76; H, 5.61; N, 13.00%); IR KBr/cm^{-1}: ν = 3447br, 1617s, 1520s, 1424s, 1091s, 801s, 622s.

$[FeC_{33}H_{45}N_7O_3]\cdot[ClO_4][Br]\cdot CH_3CN$ (2). Yellow needle crystals (66% yield); accurate ESMS (m/z): 642.2855 (20) $[Fe(L^1) - H]^+$ [calculated 642.2854]; $FeC_{35}H_{48}N_8O_3BrClO_4$ (found: C, 48.92; H, 5.54; N, 13.12% requires C, 48.71; H, 5.61; N, 12.99%); IR KBr/cm^{-1}: ν = 3445br, 1616s, 1533s, 1458s, 1443s, 1160s, 1086s, 622s; UV/Vis [λ_{max}, nm (εM, M^{-1} cm^{-1})] in CH_3CN: 321 (1180), 285 (20 380), 237 (30 170), 366 (315), 427 (220), 628 (3), 1087 (3).

$[CoC_{33}H_{45}N_7O_3]\cdot[Br]_2\cdot 0.5(H_2O)\cdot 2(CH_3CN)$ (3). Pink plate crystals (29% yield); accurate ESMS (m/z): 745.2412 (15) $[Co(L^1) + ClO_4]$ [calculated 745.2400], 645.2801 (10) $[Co(L^1) - H]^+$ [calculated 645.2837]; $CoC_{37}H_{52}N_9O_{3.50}Br_2$ (found: C, 49.66; H, 5.93; N, 14.04% requires C, 49.50; H, 5.83; N, 14.04%); IR KBr/cm^{-1}: ν = 3372s, 1618s, 1525s, 1420s, 1160s, 1097s, 622m; UV/Vis [λ_{max}, nm (εM, M^{-1} cm^{-1})] in CH_3CN: 236.2 (46 100), 285.3 (27 500), 501.5 (50), 618.4 (160), 685.5 (340).

$[NiC_{33}H_{45}N_7O_3]\cdot[ClO_4]_{1.67}[Br]_{0.33}\cdot 0.67(H_2O)$ (4). Yellow plate crystals (63% yield); accurate ESMS (m/z): 644.2885 (60) $[Ni(L^1) - H]^+$ [calculated 644.2859]; $NiC_{33}H_{46.33}Cl_{1.67}Br_{0.33}N_7O_{10.33}$; IR KBr/$cm^{-1}$: ν = 3354m, 1618s, 1531s, 1459s, 1422s, 1106s, 622s; UV/Vis [λ_{max}, nm (εM, M^{-1} cm^{-1})] in CH_3CN: 232 (26 390), 285 (15 235), 440 (30), 613 (8), 748 (7), 803 (8), 1092 (15).

$[ZnC_{33}H_{45}N_7O_3]\cdot[ClO_4]_2\cdot 2(CH_3CN)$ (5). Colourless prism crystals (89% yield); ^{1}H-NMR δ_H (400 MHz; CD_3CN): 1.14 (27H, s); 4.09 (6H, s); 7.12 (3H, d, Ar, J = 7.1 Hz); 7.21 (3H, d, Ar, J = 7.8 Hz); 7.87 (3H, t, Ar, J = 7.8 Hz); 8.98 (3H, s, NH); ^{13}C δ_C (62.5 MHz; CD_3CN): 27.0, 41.2, 55.8, 114.7, 119.9, 141.9, 153.0, 153.3, 181.3; accurate ESMS (m/z): 650.2823 (10) $[Zn(L^1) - H]^+$ [calculated 650.2797]; $ZnC_{33}H_{45}N_7O_3(CH_3CN)_2(ClO_4)_2$ (found: C, 46.93; H, 5.51; N, 13.51 requires C, 47.67; H, 5.51; N, 13.53%); IR KBr/cm^{-1}: ν = 3401br, 1617s, 1530s, 1464s, 1421s, 1120s, 1091s, 622s.

$[ZnC_{33}H_{45}N_7O_3Cl_2]$ (6). Colourless block crystals (80% yield); ^{1}H-NMR δ_H (250 MHz; DMSO): 1.34 (27H, s); 4.12 (6H, s); 7.18 (3H, d, Ar, J = 7.1 Hz); 7.49–8.31 (6H, m, Ar); 9.59 (3H, s, NH); ^{13}C-NMR δ_C (62.5 MHz; DMSO): 26.9, 54.9, 55.6, 114.8, 119.7, 140.6, 150.7, 151.0, 176.7; accurate ESMS (m/z): 650.2786 (40) $[Zn(L^1) - H]^+$ [calculated 650.2797]; $ZnC_{33}H_{45}N_7O_3(Cl)_2$ (found: C, 54.54; H, 6.27; N, 13.32% requires C, 54.90; H, 6.28; N, 13.59%). IR KBr/cm^{-1}: ν = 3426m, 1683s, 1608s, 1517s, 1455s, 1152s.

$[ZnC_{33}H_{45}N_7O_3]\cdot[ZnI_4]_{0.5}\cdot[I]$ (7). White plate crystals (63% yield); ^{1}H-NMR δ_H (250 MHz; DMSO): 1.16 (27H, s); 4.16 (6H, s); 7.24 (3H, d, Ar, J = 7.2 Hz); 7.49 (3H, d, Ar, J = 7.5 Hz); 8.07 (3H, t, Ar, J = 8.0 Hz); 10.44 (3H, s, NH); ^{13}C-NMR δ_C (62.5 MHz; DMSO): 26.5, 54.9, 55.0, 113.8, 119.0, 141.1, 151.8, 152.3, 179.9; accurate ESMS (m/z): 778.1943 (10) $[Zn(L^1) + I]^+$ [calculated 778.1920]; $ZnC_{66}H_{90}N_{14}O_6(ZnI_4)I$; IR KBr/cm^{-1}: ν = 3260m, 1615s, 1528s, 1456s, 1434s, 1417s, 1155s, 801s.

$[CdC_{33}H_{45}N_7O_3]\cdot[ClO_4]_2\cdot Na(ClO_4)\cdot H_2O$ (8). Colourless plate crystals (96% yield); ^{1}H-NMR δ_H (250 MHz; $CDCl_3$): 0.96 (27H, s); 3.76 (6H, s); 6.89 (3H, d, Ar, J = 7.5 Hz); 6.98 (3H, d, Ar, J = 8.2 Hz); 7.61 (3H, d, Ar, J = 8.0 Hz); 8.62 (3H, s, NH); ^{13}C-NMR δ_C: (62.5 MHz; CD_3CN): 27.4, 41.7, 56.7, 116.6, 121.4, 142.3, 153.5, 154.0, 183.1; accurate ESMS (m/z): 700.2570 (70), $[Cd(L^1) - H]^+$ [calculated 700.2539]; $CdC_{33}H_{45}N_7O_7NaClH_2O(ClO_4)_2$; IR KBr/cm^{-1}: ν = 3370br, 1615s, 1533s, 1454s, 1419s, 1100m, 622s.

Results and discussion

Synthesis of the ligand and complexes

Tris(6-pivaloylamino-2-pyridylmethyl)amine (TPPA) (7.272 g, 66%) was synthesised according to a literature procedure.[20] Initial attempts to obtain crystals of complexes of L^1 were only successful for $Zn(ClO_4)_2$ and $Cd(ClO_4)_2$. However, on using the protonated ligand $[HL^1][Br]$ we were able to obtain single crystals for Mn^{II}, Fe^{II}, Co^{II} and Ni^{II} complexes. However, using this ligand combination with $Zn(ClO_4)_2$ did not yield a crystalline species. With this in mind, further investigations were carried out with the Zn^{II} species by using different starting materials, $ZnCl_2$ and ZnI_2. The complexation involved the use of either ligand L^1 or $[HL^1][Br]$ (1 equivalent, typically 0.085 mmol) which was dissolved in the minimum amount of warm acetonitrile. The metal salt (1 equivalent) was dissolved in acetonitrile and added dropwise. The compound was isolated by crystallisation through diffusion of diethyl ether vapour into the acetonitrile reaction mixture. On some occasions (Mn(II), Fe(II)), slow evaporation was used to obtain crystals. The yields from these reactions ranged from moderate to good (25–97%), though, of course, this reflects the amount of product that precipitated from solution, not the yield of product from the initial reaction. The crystalline material was subsequently used for all spectroscopic measurements.

Spectroscopic properties of complexes

IR spectra. The free ligand reveals a very strong single band at 1691 cm^{-1}, assigned to the ν(C═O) vibration of the three equivalent amide carbonyl groups (Table 1). This signal is observed at lower energy in all complexes upon co-ordination to the metal. For complex **6**, although the solid state structure shows two carbonyl environments, neither are directly co-ordinated to the metal centre, though two amides form strong hydrogen bonds to the co-ordinated chlorides. Interestingly, only one carbonyl stretch is observed at 1683 cm^{-1}. Similarly, Mareque Rivas observed the carbonyl stretch of the amide in bppapa, hydrogen bonded to the Zn–Cl moiety at 1700 cm^{-1}.[21]

Table 1 IR stretching frequencies of L^1 (cm^{-1})

Compound	ν(C═O)	ν(Cl–O)
L^1	1691(s)	—
1	1617(s)	1091(m), 622(s)
2	1616(s)	1086(m), 622(s)
3	1618(s)	1097(s), 622(m)
4	1618(s)	1106(m), 622(s)
5	1617(s)	1091(s), 622(s)
6	1683(s)	—
7	1615(s)	—
8	1615(s)	1100(m), 622(s)

IR spectra measured as KBr discs.

Compounds **1–5** and **8** reveal two characteristic unsplit infrared active bands at ~1100 cm^{-1} and 622 cm^{-1} indicative of ionic perchlorate (T_d symmetry).[22,23] This is confirmed by X-ray diffraction studies.

Cyclic voltammetry

The cyclic voltammogram of the manganese compound, **1**, reveals three irreversible oxidations within the anodic region at +0.420, +0.708 and +1.17 V (*vs.* Fc^+/Fc). In comparison, the seven co-ordinate manganese(II) complex of *N*,*N*,*N*′-tris(2-pyridylmethyl)-*N*′-(2-salicylideneethyl)ethane-1,2-diamine and Mn^{II}(pyrdoxTPA)$_2$ reveals a Mn(II/III) redox process at +0.10 V and +0.18 V (*vs.* Fc^+/Fc) respectively (Table 2).[24–26]

The cyclic voltammogram of **2** exhibits a quasi-reversible wave at +0.253 V (*vs.* Fc^+/Fc) which has been ascribed to the Fe(II/III) redox couple. The separation between the anodic and cathodic peaks, $E_p^c - E_p^a$, is 140 mV (significantly larger than the 80 mV observed for the internal standard). The compound $[Fe(k^7N\text{–}L](ClO_4)_2$ L = *N*,*N*,*N*′,*N*′-tetrakis(2-pyridylmethyl)-2,6-bis(aminomethyl)pyridine also exhibits a seven-coordinate environment around the Fe(II) ion and also reveals a quasi-reversible Fe(II)/Fe(III) couple at the higher potential of +0.51 V *vs.* Fc^+/Fc[27] which surprisingly suggests that L^1 leads to a more electron rich metal centre in **2**.

The cyclic voltammogram of the cobalt(II) complex, **3**, reveals a quasi-reversible redox process in the anodic region at +0.588 V (65) which has been tentatively assigned to the Co(II)/

Table 2 Electrochemical parameters for the redox processes exhibited by complexes **1**, **2**, **3** and **4** in acetonitrile solution (supporting electrolyte: $[Bu_4N][PF_6]$ (0.1 mol dm^{-3}); T = 20 °C). Measured at 0.1 V s^{-1}

Compound	E_p/V (ΔE, mV)[a,b]
1	0.420, 0.708, 1.17
2	0.253(140)
3	0.354, 0.588(65)
4	−2.14

[a] The potentials at which reversible processes occur are calculated as the average of the oxidative and reductive peak potentials $(E_p^{ox} + E_p^{red})/2$. [b] For irreversible processes, the anodic or cathodic peak potentials are given. Potentials are given in volts *versus* ferrocenium/ferrocene.

Co(III) couple. There is also a further irreversible oxidation at +0.354 V.

No reversible processes are observed in the cyclic voltammogram of the nickel compound **4**. Only one irreversible reduction at −2.14 V (*vs.* Fc^+/Fc) is seen.

Electronic absorption spectra

The electronic spectra of L^1 and its complexes have been measured and the data are presented in Table 3. All measurements were recorded from an acetonitrile solution of the respective complex. The free ligand shows typical π–π* transitions at high energy (243, 284 and 320 nm). Each of the complexes, **2–4**, also reveals π–π* transitions at similar energy to those of the free ligand.

The electronic spectrum of compound **2** reveals two MLCT transitions at 27 325 and 23 420 cm^{-1} and two d–d transitions within the visible region at 15 925 and 9200 cm^{-1}, assuming a high spin co-ordination environment in solution. The observation of two (rather than one observed in octahedral complexes) is consistent with the lower C_{3v} symmetry of a capped octahedron, which results in the splitting of the T_{2g} term into an A and an E term.

The Co^{II} complex **3** has also been shown to contain a seven-coordinate environment around the metal centre and its absorption spectrum consists of three absorptions at 19 940, 16 170 and 14 590 cm^{-1}. While a seven co-ordinate species will in theory show extensive splitting of the free ion F terms (to $2A_2$, A_1 and 2E) and P terms (to A_2 and E), the observed spectrum suggests that the splitting is small and best approximated to an octahedral geometry. However, the lowest energy transition is significantly higher than that observed for most octahedral Co(II) complexes[28] and it is likely that the first transition was not observed in the available spectral range (300–1100 nm).

The UV spectrum of Ni^{II}, **4**, reveals two LMCT bands observed at 22 730 and 16 300 cm^{-1}. In the solid state, the Ni^{II} cation lies at the centre of an N_4O_3 coordination environment of a mono capped octahedral geometry. The absorption pattern is at first glance indicative of an octahedral geometry in solution. Four transitions are observed at 16 300, 13 370, 12 450 and 9160 cm^{-1} which suggest transitions from $^3A_{2g}$ to $^3T_{1g}(P)$, $^3T_{1g}(F)$, ^1E_g and $^3T_{2g}$, respectively. However, caution should be applied as, if Δ and B are calculated utilising the first two spin allowed transitions, the values obtained are not consistent with the energy of the third spin allowed transition. Therefore it seems likely that the spectrum reflects a lower symmetry than O_h.

Table 3 Electronic spectral assignments for the ligand and complexes[a]

Compound	π–π* λ (nm)	MLCT λ (nm)	d–d λ (nm)
L^1	243(21 870) 284(17 920) 320(1810)	—	—
2	237(30 170) 285(20 380) 321(1180)	366(315) 427(220)	628(3) 1087(3)
3	236.2(46 100) 285.3(27 500)	—	501.5(50), 618.4(160), 685.5(340)
4	232(26 390) 285(15 235)	440(30)	613(8), 748(7) 803(8) 1092(15)

[a] Performed in a CH_3CN solution at room temperature; numbers in parentheses indicate molar absorption coefficients ε (M^{-1} cm^{-1}).

Crystallographic studies

All single crystal X-ray data were collected on a Bruker/Nonius Kappa CCD diffractometer using graphite monochromated Mo-Kα radiation (λ = 0.71073 Å), equipped with an Oxford Cryostream cooling apparatus. Crystal parameters and details of the data collection, solution and refinement are presented in Table 4. The data were corrected for Lorentz and polarization effects and for absorption using SORTAV.[29] Generally structure solution was achieved by direct methods (the Sir-92 program system)[30] and refined by full-matrix least-squares on F^2 (SHELXL-97)[31] with all non-hydrogen atoms assigned anisotropic displacement parameters. Hydrogen atoms attached to carbon atoms were placed in idealised positions and allowed to ride on the relevant carbon atom. In the final cycles of refinement, a weighting scheme that gave a relatively flat analysis of variance was introduced and refinement continued until convergence was reached. Molecular structures in the figures were drawn with ORTEP-3.0 for Windows (version 2.02).[32] The metal co-ordination geometry is given for all structures in Table 5. Continuous shape mapping (CShM) was used to calculate the deviation in the core geometry of crystal structures.[33] Unfortunately, only poor quality crystals could be obtained for $[NiL^1][Br][ClO_4]$, despite numerous attempts to grow better crystals.

$[Mn^{II}(L^1)][ClO_4][Br]\cdot CH_3CN$ (1). The manganese compound crystallises in the monoclinic space group $P2_1/m$ and contains one complex within the asymmetric unit (asu) (Fig. 2). The Mn^{II} ion lies at the centre of a slightly distorted capped octahedron co-ordination geometry which has been confirmed by CShM (Table 6). The Mn^{II} ion is surrounded by two types of donor atoms. There are four N-donors N1, N2, N4 and N6 and three oxygen donors O1, O2 and O3 (Fig. 3). The co-ordinative bond lengths range from 2.161(3) Å to 2.316(4) Å. The co-ordinative bond lengths of nitrogen donors N1, N2, N4 and N6 (Table 5) are slightly shorter than those of the seven coordinate compound $[Mn^{II}(TPA)][NO_3]_2$ (TPA = tris(2-pyridylmethyl)-amine) which ranges from 2.2616(16) Å for the pyridyl donors to 2.3889(16) Å for the central nitrogen donor.[34] This may reflect the steric constraints of L^1, which leads to closer contact between the metal and the ligand.

$[Fe^{II}(L^1)][ClO_4][Br]\cdot CH_3CN$ (2). The iron compound crystallises in the monoclinic space group $P2_1/m$ and contains one complex within the asu. Similar to the Mn(II) complex, the Fe^{II} is co-ordinated *via* four N-donors and three oxygen donors. Again, the core geometry is best described as a capped octahedron, with S(OCF) and S(TPRS) values of 0.335 and 1.498, respectively (Table 6). The co-ordinative bond lengths are

Table 4 Crystal structure data for complexes **1–8**

Compound	**1**	**2**	**3**	**4**	**5**	**6**	**7**	**8**
Chemical formula	$MnC_{36}H_{49.5}N_{8.5}O_7BrCl$	$FeC_{35}H_{48}N_8O_7BrCl$	$CoC_{37}H_{52}N_9O_{3.50}Br_2$	$NiC_{33}H_{46.33}Br_{0.33}N_7Cl_{1.67}O_{10.33}$	$ZnC_{37}H_{51}N_9O_{11}Cl_2$	$ZnC_{33}H_{45}N_7O_3Cl_2$	$Zn_3C_{66}H_{90}N_{14}O_6I_6$	$CdC_{33}H_{47}N_7O_{16}NaCl_3$
M_r (g mol^{-1})	883.64	864.02	897.63	850.87	934.14	724.03	2133.03	1039.52
Crystal system	Monoclinic	Monoclinic	Monoclinic	Hexagonal	Monoclinic	Monoclinic	Trigonal	Trigonal
Space group	$P2_1/m$	$P2_1/m$	$C2/c$	$P6_3/m$	$C2/c$	$C2/c$	$P\bar{3}c1$	$R32$
T (K)	150(2)	150(2)	150(2)	396(2)	150(2)	140(2)	150(2)	150(2)
a (Å)	10.8160(2)	10.730(5)	11.1532(3)	11.1018(7)	37.4589(10)	35.4990(4)	11.2190(2)	16.2935(5)
b (Å)	40.8620(8)	40.995(5)	19.6165(5)	11.1018(7)	11.2206(3)	9.1250(7)	11.2190(2)	16.2935(5)
c (Å)	11.1620(2)	11.101(5)	37.6128(12)	58.814(4)	21.1473(8)	24.5700(12)	38.5920(4)	28.8420(13)
α (°)	90	90	90	90	90	90	90	90
β (°)	116.9550(10)	117.050(5)	90.6930(10)	90	93.2280(10)	119.271(2)	90	90
γ (°)	90	90	90	120	90	90	120	120
Z	4	4	8	6	8	8	2	6
D_c (Mg m^{-3})	1.335	1.320	1.449	1.375	1.398	1.385	1.684	1.562
μ(Mo Kα) (mm^{-1})	1.322	1.378	2.407	0.875	0.740	0.906	3.102	0.760
Collected reflections	14 579	10 265	13 749	2176	29 824	16 682	22 993	6695
Unique reflections	8298	7092	7535	1987	10 144	6270	3221	2772
R_{int}	0.0460	0.0477	0.0453	0.0735	0.1050	0.0696	0.0737	0.0821
R_1 [$I > 2\sigma(I)$]	0.0619	0.0769	0.04256	0.2730	0.0779	0.0765	0.0456	0.1023
wR_2 (all data)	0.1478	0.1749	0.0883	0.6453	0.1842	0.1891	0.1154	0.2514

shorter than those observed for Mn(II) and range from 2.132(5) Å to 2.257(5) Å (Table 5). These values are similar to those observed for the 7-coordinate complex, $[Fe(H_2bppa)(HCOO)]^{2+}$ (bppa = bis(6-pivalamido-2-pyridylmethyl)(2-pyridylmethyl)-amine), reported by Wada *et al.* where the Fe–N bond lengths range between 2.004(3) Å and 2.226(3) Å.[35]

$[Co^{II}(L^1)][Br]_2\cdot0.5(H_2O)\cdot2(CH_3CN)$ (3). The cobalt compound crystallises in the monoclinic space group $C2/c$ and contains one complex within the asu (Fig. 4). There are four nitrogens and three oxygens within the co-ordinative sphere of the central Co(II) ion. In an attempt to grow crystals of **3**, the perchlorate salt was used with no success. However, crystals were obtained by using $HBrL^1$. The co-ordination geometry of the Co^{II} ion is best described as a capped octahedron similar to all other structures (except compound **6**). This is the first example of Co^{II} being seven coordinate in a TPA based ligand.

$[Ni^{II}(L^1)][ClO_4]_{1.67}[Br]_{0.33}\cdot0.67(H_2O)$ (4). The nickel compound crystallises in the hexagonal space group $P63/m$ and contains two unique complexes within the asu, of which one is disordered. Unfortunately, due to this disorder and the poor quality of the obtained crystals the solution to this structure has a high R factor, with the exact location of two counter-ions and a solvent molecule being unclear. However, the general co-ordination mode of the ligand to the nickel centre in one complex is well determined. In an analogous manner to the Mn^{II} (**1**) and Fe^{II} (**2**) complexes, the Ni^{II} ion is coordinated by four N-donors and three O donors (Fig. 5 and 6). The co-ordinative bond lengths are typical with the exception of the long Ni^{II}–N1 bond (Table 5). This long bond perhaps reflects the tendency of Ni^{II} towards a six co-ordinate octahedral geometry, and of the seven co-ordinate structures formed by L^1, the nickel complex shows the greatest deviation from both mono capped octahedral and mono capped trigonal prismatic seven co-ordinate geometries, towards the six co-ordinate octahedral geometry.

$[Zn^{II}(L^1)][ClO_4]_2\cdot2(CH_3CN)$ (5). The zinc compound crystallises in the monoclinic space group $C2/c$ and contains one complex within the asu (Fig. 7). The Zn(II) cation lies at the centre of a capped octahedral geometry (Table 6). There are four nitrogen donors (N1, N2, N3 and N4) and three oxygen donors (O1, O2 and O3) (Fig. 8). All four M–N bond lengths are very similar in length and vary from 2.182(4) Å to 2.244(5) Å. This is longer than those found in $[Zn^{II}(TPA)Cl]Cl$[36] which range from 2.062(2) to 2.083(2) Å for the M–N pyridyl bonds. All three oxygen donors are slightly shorter and range between 2.137(3) Å and 2.149(3) Å. The structure is similar to those observed with Mn(II), Fe(II), Co(II) and Zn(II) (**7**).

$[Zn^{II}(L^1)(Cl)_2]$ (6). Compound (**6**) was synthesised by the reaction of L^1 with $ZnCl_2$. The zinc compound crystallises in the monoclinic space group $C2/c$ and contains one complex within the asu (Fig. 9). The Zn(II) cation lies at the centre of a slightly distorted trigonal bipyramidal geometry (Tables 7 and 8). There are three nitrogen donors (N1, N2 and N4), two of which are pyridyl groups, the other being an aliphatic nitrogen donor (N1). The aliphatic nitrogen donor and two chloride donors occupy the equatorial positions. One arm of TPPA does not

Table 5 Crystal structure data for complexes **1–5** and **7**

	$[MnL^1]^{2+}$ **1**	$[FeL^1]^{2+}$ **2**	$[CoL^1]^{2+}$ **3**	$[NiL^1]^{2+}$ **4**	$[ZnL^1]^{2+}$ **5**	$[ZnL^1]^{2+}$ **7**	$[CdL^1]^{2+}$ **8**
M(1)–N(1)	2.264(4)	2.220(6)	2.184(3)	2.53(2)	2.221(4)	2.180(6)	2.354(12)
M(1)–N(2)	2.309(4)	2.256(5)	2.217(3)	2.264(7)	2.244(5)	2.233(4)	2.362(5)
M(1)–N(4)	2.316(4)	2.257(5)	2.236(3)	2.264(7)	2.182(4)	2.233(4)	2.362(5)
M(1)–N(6)	2.309(4)	2.256(6)	2.205(3)	2.264(7)	2.205(4)	2.233(4)	2.362(5)
M(1)–O(1)	2.173(3)	2.143(5)	2.143(2)	2.033(11)	2.148(4)	2.127(3)	2.249(8)
M(1)–O(2)	2.161(3)	2.158(5)	2.119(2)	2.033(11)	2.149(3)	2.127(3)	2.249(8)
M(1)–O(3)	2.185(3)	2.132(5)	2.114(2)	2.033(11)	2.137(3)	2.127(3)	2.249(8)
N(1)–M(1)–N(2)	73.18(14)	73.2(2)	73.71(10)	70.3(2)	73.44(19)	73.98(9)	71.88(11)
N(1)–M(1)–N(4)	71.78(14)	73.0(2)	73.03(9)	70.3(2)	74.42(15)	73.98(9)	71.88(11)
N(1)–M(1)–N(6)	72.02(14)	73.0(2)	74.42(10)	70.3(2)	73.57(17)	73.98(9)	71.88(11)
N(2)–M(1)–N(4)	111.38(14)	113.0(2)	112.58(10)	109.3(2)	110.18(15)	112.69(7)	110.79(11)
N(2)–M(1)–N(6)	113.29(14)	112.7(2)	111.48(10)	109.3(2)	113.27(16)	112.69(7)	110.79(11)
N(6)–M(1)–N(4)	108.96(14)	109.86(19)	113.33(10)	109.3(2)	114.16(16)	112.69(7)	110.79(11)
O(1)–M(1)–N(1)	130.36(14)	131.6(2)	130.50(9)	128.2(4)	132.12(16)	129.48(9)	126.7(2)
O(1)–M(1)–N(2)	76.88(13)	78.81(19)	78.89(9)	81.9(4)	78.98(17)	78.34(12)	73.5(4)
O(1)–M(1)–N(4)	157.51(14)	83.22(19)	156.47(9)	79.0(4)	79.60(14)	79.12(12)	159.5(4)
O(1)–M(1)–N(6)	85.07(14)	155.3(2)	78.56(9)	161.8(5)	154.28(15)	156.54(13)	84.5(5)
O(1)–M(1)–O(3)	85.04(13)	83.78(19)	85.26(9)	86.4(6)	81.63(14)	83.89(13)	87.9(3)
O(2)–M(1)–O(1)	84.92(13)	82.54(18)	83.15(9)	86.4(6)	83.62(14)	83.89(13)	87.9(3)
O(2)–M(1)–N(1)	126.19(14)	130.31(18)	129.92(10)	128.2(4)	128.92(16)	129.48(9)	126.7(2)
O(2)–M(1)–N(2)	79.75(13)	156.5(2)	80.18(9)	161.8(5)	157.64(16)	156.54(13)	85.5(5)
O(2)–M(1)–N(4)	76.44(13)	78.44(18)	78.96(9)	81.9(4)	80.01 (14)	78.34(13)	73.5(4)
O(2)–M(1)–O(3)	86.29(13)	85.22(18)	84.46(9)	86.4(6)	85.05(13)	83.89(13)	87.9(3)
O(2)–M(1)–N(6)	161.19(14)	79.91(19)	155.66(10)	79.0(4)	77.97(14)	79.12(12)	159.5(4)
O(3)–M(1)–N(1)	128.76(14)	126.6(2)	127.22(10)	128.2(4)	128.34(14)	129.48(9)	126.7(2)
O(3)–M(1)–N(2)	157.98(14)	78.7(2)	159.07(10)	79.0(4)	78.65(15)	79.12(12)	159.5(4)
O(3)–M(1)–N(4)	81.34(14)	160.3(2)	77.94(9)	161.8(5)	157.12(15)	156.54(13)	85.5(5)
O(3)–M(1)–N(6)	77.00(13)	77.6(2)	78.18(9)	81.9(4)	79.06(14)	78.34(13)	72.5(4)

For convenience, the following labels in the table should be replaced with those indicated for the corresponding metal complexes: For Ni(**4**), Zn(**7**) and Cd(**8**): N(4) = N(2)#1, N(6) = N(2)#2, O(2) = O(1)#1, O(3) = O(1)#2. For Zn(**5**): N(4) = N(3), N(6) = N(4). Symmetry operations represented by #1 and #2 are unique for each complex.

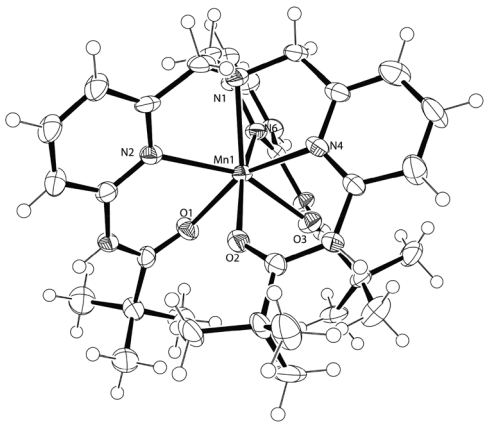

Fig. 2 The asymmetric unit of **1**. Displacement ellipsoids are shown at 50% probability. H atoms are of arbitrary size.

co-ordinate to the metal centre (Fig. 10). The co-ordinative bond lengths are typical of nitrogen donors and vary from 2.139(5) Å to 2.233(5) Å (Table 7) and again are similar to the compound $[Zn^{II}(TPA)Cl]Cl$.[36]

Hydrogen bond interactions are observed between $H_{3a}\cdots Cl_1$ and $H_{5a}\cdots Cl_1$ (Fig. 11) with bond lengths 2.637, 2.618 Å respectively. A weaker hydrogen bond is observed between $H_{3a}\cdots Cl_2$ (3.208 Å). Previously, Mareque Rivas[18] has shown how the formation of a CuL^1Cl complex is stabilised by effective hydrogen bonding between the amide H-bond donor and the chloride. Surprisingly, in this case both chloride atoms co-ordinate to the metal leaving one arm of the ligand free. This might suggest that in the solid state for zinc, with no strong LFSE, there is no strong preference for a particular ligand set and strong hydrogen bonding interactions lead to both chlorides co-ordinating to the metal centre, each supported by an interaction with an amido group.

$[Zn^{II}(L^1)][ZnI_4]_{0.5}[I]$ (7). From the reaction of ZnI_2 with L^1, the resulting zinc compound crystallises in the trigonal space group $P\bar{3}c1$ and contains one complex within the asu (Fig. 12). In the structure, there are two types of anionic counter-ions: a simple iodide anion and the dianion, $[ZnI_4]^{2-}$. There is one $[ZnI_4]^{2-}$ counter-ion for every two cationic species, and the $[ZnI_4]^{2-}$ species was found to be disordered within the lattice. Similar to **5** the metal ion lies within a slightly distorted capped octahedron (Table 6), although the complex now has threefold symmetry with all pyridyl donors and oxygen donors being symmetrically equivalent (Fig. 13). Comparison between complexes **5** and **7** shows very similar bond lengths and angles.

$[Cd^{II}(L^1)][ClO_4]_2\cdot Na(ClO_4)\cdot H_2O$ (8). The cadmium compound crystallises in the trigonal space group *R*32 and contains one complex within the asu (Fig. 14). The cadmium complex again has a seven co-ordinated, capped-octahedral geometry (Table 6). Unexpectedly, in the crystals obtained, a sodium perchlorate molecule co-crystallised. The sodium

Table 6 Continuous symmetry mapping results of seven coordinate complexes show strong preferences of a mono capped octahedron

	Compound						
Geometry	**1**	**2**	**3**	**4**	**5**	**7**	**8**
Heptagon	35.93	35.63	36.22	36.52	35.78	36.64	36.53
Hexagonal pyramid	20.02	20.40	19.78	19.60	20.18	19.79	19.29
Pentagonal bipyramid	7.84	7.68	7.75	8.75	7.79	8.28	8.53
Capped octahedron	0.33	0.34	0.23	0.53	0.29	0.24	0.48
Capped trigonal prism	1.53	1.50	1.48	2.02	1.25	1.64	1.89
Johnson pentagonal bipyramid J13	11.67	11.42	11.49	12.08	11.37	12.05	12.40
Johnson elongated triangular pyramid J7	18.85	19.44	20.31	18.05	19.69	20.19	17.31

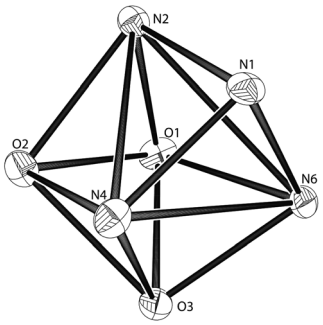

Fig. 3 A view of the core geometry of **1** of covalent bond radius less than 3 Å. The metal has been removed to help illustrate the geometry.

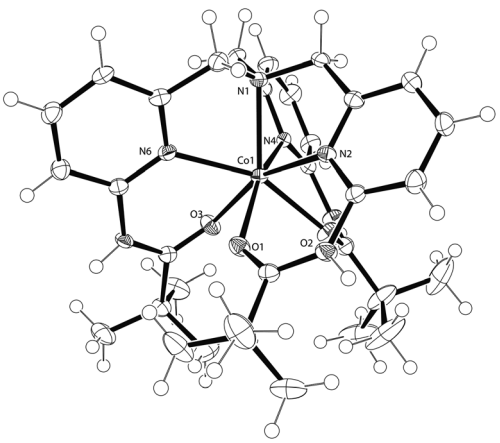

Fig. 4 The asymmetric unit of **3**. Displacement ellipsoids are shown at 50% probability. H atoms are of arbitrary size.

counter-ion was an impurity in the ligand starting material, included with the ligand when it was dried with sodium sulphate. Again, as seen in **4** and **7**, there is threefold symmetry about the N(1)–M bond, making the three M–pyridine bond equivalent. The metal–donor bond lengths observed in this complex are similar to those observed in related species; for example in $[Cd^{II}(TPA)(NO_3)(H_2O)]\cdot NO_3$[3] the N–$Cd^{II}$ bond lengths vary from 2.30(1) Å to 2.44(1) Å.

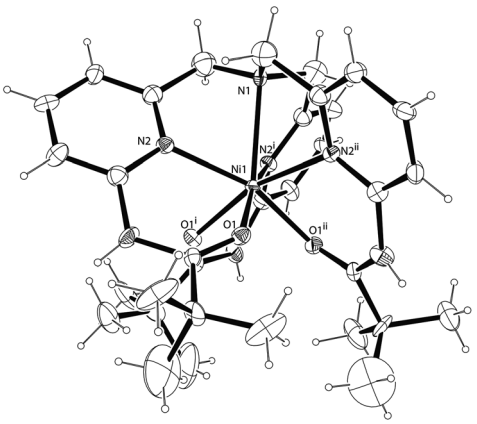

Fig. 5 The asymmetric unit of **4**. Displacement ellipsoids are shown at 10% probability. H atoms are of arbitrary size.

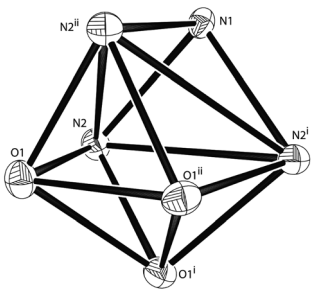

Fig. 6 A view of the core geometry of **4** of covalent bond radius less than 3 Å. The metal has been removed to help illustrate the geometry.

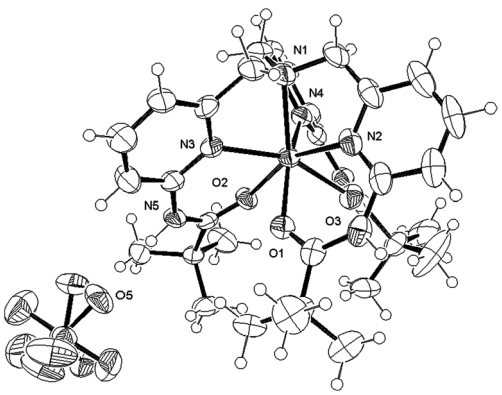

Fig. 7 The asymmetric unit of **5**. Displacement ellipsoids are shown at 50% probability. H atoms are of arbitrary size.

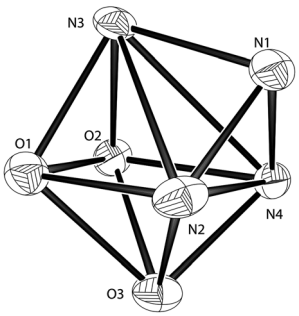

Fig. 8 A view of the core geometry of **5** of covalent bond radius less than 3 Å. The metal has been removed to help illustrate the geometry.

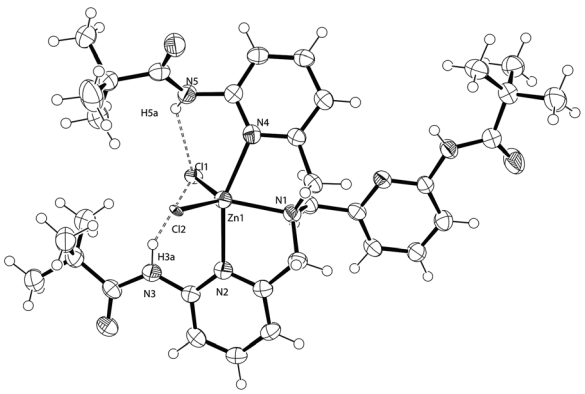

Fig. 9 The asymmetric unit of **6**. Displacement ellipsoids are shown at 50% probability. H atoms are of arbitrary size.

Table 7 Selected bond lengths (Å) and angles (°) for $[ZnL^1Cl_2]$ **6**

Zn(1)–N(1)	2.138(5)	Zn(1)–Cl(1)	2.3033(15)
Zn(1)–N(2)	2.228(5)	Zn(1)–Cl(2)	2.3327(13)
Zn(1)–N(4)	2.209(5)		
N(1)–Zn(1)–N(2)	78.53(18)	N(2)–Zn(1)–Cl(2)	93.21(13)
N(1)–Zn(1)–N(4)	78.31(18)	N(4)–Zn(1)–N(2)	156.82(18)
N(1)–Zn(1)–Cl(1)	116.78(14)	N(4)–Zn(1)–Cl(1)	94.60(13)
N(1)–Zn(1)–Cl(2)	123.81(14)	N(4)–Zn(1)–Cl(2)	99.04(14)
N(2)–Zn(1)–Cl(1)	96.42(13)	Cl(1)–Zn(1)–Cl(2)	119.36(5)

Table 8 Continuous shape mapping results for complexes **6**

Structure	(PP)	(VOC)	(TBPY)	(SPY)	(JSPY)	(JTBP)
L^1_Zn(**6**)	33.350	6.694	1.465	4.061	6.694	4.969

PP: pentagon (D_{5h}), VOC: vacant octahedron (C_{4v}), TBPY: trigonal bipyramid (D_{3h}), SPY: square pyramid (C_{4v}), JSPY: Johnson square pyramid (C_{4v}), JTBP: Johnson trigonal bipyramid (D_{3h}).

Structural analysis

Continuous shape mapping (CShM) quantifies the shape of a co-ordination geometry when compared to idealised polyhedra. It allows the identification of any distortion from the idealised geometry and the *S* value for a given geometry is a measure of how close it is to a given idealised geometry. Near-perfect shapes will have an *S* value close to zero and geometries which depart significantly from a perfect polyhedron will have higher *S* values. Table 6 lists the shape values for complexes **1–5**, **7** and **8** for the various seven vertices structures.

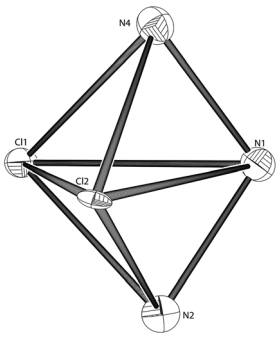

Fig. 10 A view of the core geometry of **6** of covalent bond radius less than 3 Å. The metal has been removed to help illustrate the geometry.

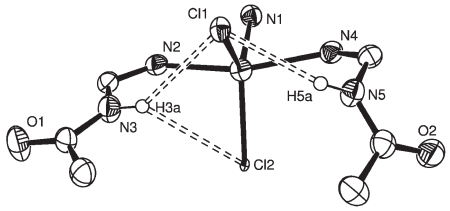

Fig. 11 A view of the hydrogen bonding interactions of **6**.

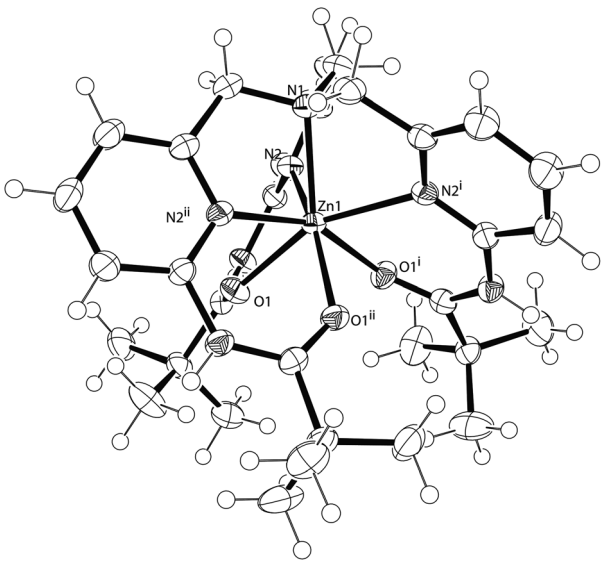

Fig. 12 The asymmetric unit of **7**. Displacement ellipsoids are shown at 50% probability. H atoms are of arbitrary size.

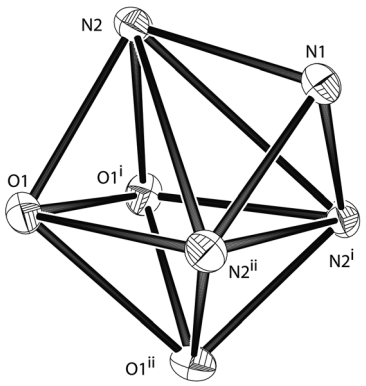

Fig. 13 A view of the core geometry of **7** of covalent bond radius less than 3 Å. The metal has been removed to help illustrate the geometry.

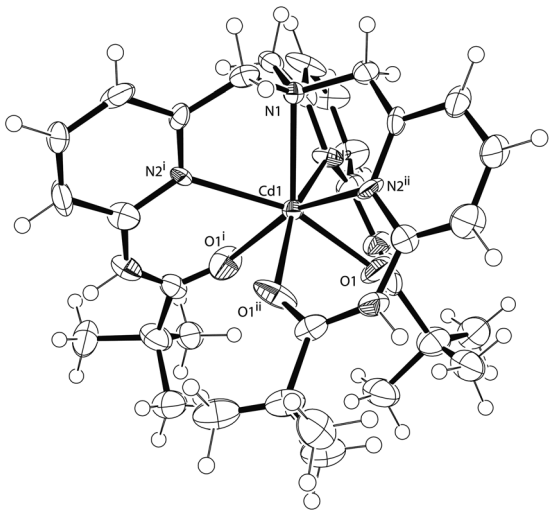

Fig. 14 The asymmetric unit of **8**. Displacement ellipsoids are shown at 50% probability. H atoms are of arbitrary size.

Conclusions

A series of transition metal complexes with a trisamide ligand based on a TPA framework have been synthesised and structurally characterised. This ligand readily forms seven co-ordinate complexes when no additional potential ligands are present. However, in the case of **6**, a five coordinate trigonal bipyramidal geometry is preferred due to the co-ordination of chloride anions to the metal centre. This formation of a five co-ordinate species in the presence of the chloride anion shows how the resulting co-ordination environment seems to be dependent on the identity of the counter-ion and suggests that the donor strength of the carbonyl in L^1 is intermediate to chloride and bromide. In fact, bromide, iodide and perchlorate are all weaker donors than the carbonyl and result in seven co-ordinate structures. In addition, the ability of ternary ligands to bind to ML^1 may also be modified by the ternary ligand's ability to hydrogen bond to L^1 upon co-ordination to the metal.

With the exception of the five co-ordinate complex, **6**, all the seven co-ordinate structures are best described as having a capped octahedral metal centre, though the shape analysis highlights how closely related the MCO and MCTP geometries are.

Table 9 A comparison between θ_2 and θ_5 averaged angles for the structures and their relationship with Hoffman's angles

	θ_2	θ_5
Ideal	54.7°	125.3°
Hoffman ideal	75°	138°
Mn^{II} (1)	72.4°	128.5°
Fe^{II} (2)	73.7°	129.2°
Co^{II} (3)	73.1°	129.6°
Ni^{II} (4)	70°	128°
Zn^{II} (5)	73.9°	129.8°
Zn^{II} (7)	73.9°	129.5°
Cd^{II} (8)	71.9°	126.6°

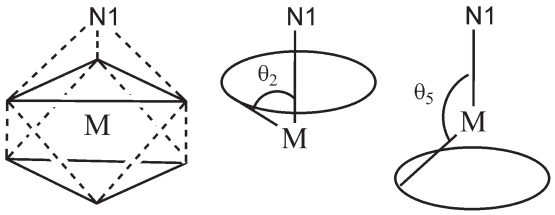

Fig. 15 θ_2 and θ_5 in a mono capped octahedron.

Table 9 shows the angles θ_2 and θ_5 (see Fig. 15) for all mono capped octahedron structures in relation to the ideal and Hoffman ideal angles.[37] In this model, θ_2 is the N–M–N angle between the capping N, the metal centre and any of the next three nearest N atom donors. θ_5 is the N–M–N angle between the capping N donor and the furthest three N donors.

It would appear that the ML^1 structures are sterically constrained and all angles lie between the ideal CO and Hoffman ideal angles.[37] In addition, due to the long bond for Ni–N1, in comparison to all other M–N1 bonds, we can see that θ_2 (N1–Ni–N2, N1–Ni–N4, N1–Ni–N6) is relatively acute compared to θ_2 in the other complexes; however, in general terms, it is interesting to note that such a different structure only produces a ~3–4° change in angle when compared to the other late transition metal ions, while the larger cations, Mn(II) and Cd(II), are different again and the angles lie between those observed for nickel and the other metals.

Finally, a CCDC database search shows how rare this coordination number is for transition metal complexes. For example, among all manganese structures only 6.1% are seven coordinate, iron ~4.0%, cobalt ~2.3%, nickel ~0.7%, zinc ~0.4%, and cadmium ~7.3%. This tripodal ligand favours the formation of seven co-ordinate capped octahedral complexes when no additional ligands are present. Such geometries are extremely rare and more typically seen in complexes of the larger cations, such as Mn(II) and Cd(II). It is particularly unusual to observe seven co-ordinate structures of Ni(II) and Zn(II). The crystallographic data highlight how the pre-organisation of the ligand leads to what may typically be regarded as an unfavourable geometry of the transition metal ions and the

formation of seven co-ordinate species with labile amide donors may be useful for the formation of catalyst precursors.

Acknowledgements

We wish to thank Dr R. J. Jenkins and R. Hicks for performing the mass spectrometry experiments. We also thank Umm Al-Qura University of the Kingdom of Saudi Arabia for financial support.

References

1 G. Anderegg and F. Wenk, *Helv. Chim. Acta*, 1967, **50**, 2330.
2 A. Hazell, K. B. Jensen, C. J. McKenzie and H. Toftlund, *Inorg. Chem.*, 1994, **33**, 3127.
3 C. S. Allen, C.-L. Chuang, M. Cornebise and J. W. Canary, *Inorg. Chim. Acta*, 1995, **239**, 29–37.
4 B. G. Gafford and R. A. Holwerda, *Inorg. Chem.*, 1989, **28**, 60.
5 C. X. Zhang, S. Kaderli, M. Costas, E. Kim, Y.-M. Neuhold, K. D. Karlin and A. D. Zuberbühler, *Inorg. Chem.*, 2003, **42**, 1807.
6 A. Diebold and K. S. Hagen, *Inorg. Chem.*, 1998, **37**, 215.
7 D. G. Lonnon, D. C. Craig and S. B. Colbran, *Dalton Trans.*, 2006, 3785.
8 Z. H. Zhang, X. H. Bu, Z. A. Zhu and Y. T. Chen, *Polyhedron*, 1996, **15**, 2787.
9 J. Bjernemose, A. Hazell, C. J. McKenzie, M. F. Mahon, L. P. Nielsen, P. R. Raithby, O. Simonsen, H. Toftlund and J. A. Wolny, *Polyhedron*, 2003, **22**, 875.
10 A. Diebold and K. S. Hagen, *Inorg. Chem.*, 1998, **37**, 215.
11 Y. Gultneh, A. Farooq, K. D. Karlin, S. Liu and J. Zubieta, *Inorg. Chim. Acta*, 1993, **211**, 171.
12 Z. He, D. C. Craig and S. B. Colbran, *Dalton Trans.*, 2002, 13.
13 Z. He, P. J. Chaimungkalanont, D. C. Craig and S. B. Colbran, *Dalton Trans.*, 2000, 1419.
14 Y. Zang, J. Kim, Y. H. Dong, E. C. Wilkinson, E. H. Appelman and L. Que, *J. Am. Chem. Soc.*, 1997, **119**, 4197.
15 H. Hayashi, S. Fujinami, S. Nagatomo, S. Ogo, M. Suzuki, A. Uehara, Y. Watanabe and T. Kitagawa, *J. Am. Chem. Soc.*, 2000, **122**, 2124.
16 H. Hayashi, K. Uozumi, S. Fujinami, S. Nagatomo, K. Shiren, H. Furutachi, M. Suzuki, A. Uehara and T. Kitagawa, *Chem. Lett.*, 2002, 416.
17 C.-l. Chuang, K. Lim, Q. Chen, J. Zubieta and J. W. Canary, *Inorg. Chem.*, 1995, **34**, 2562.
18 J. C. Mareque Rivas, S. L. Hinchley, L. Metteau and S. Parsons, *Dalton Trans.*, 2006, 2316; D. Natale and J. C. Mareque Rivas, *Chem. Commun.*, 2008, 425.
19 S. Yamaguchi, A. Wada, Y. Funahashi, S. Nagatomo, T. Kitagaw, K. Jitsukawa and H. Masuda, *Eur. J. Inorg. Chem.*, 2003, 4378.
20 M. Harata, K. Jitsukawa, H. Masuda and H. Einaga, *Chem. Lett.*, 1995, 61.
21 J. C. Mareque Rivas, R. T. Martin de Rosales and S. Parsons, *Dalton Trans.*, 2003, 2156.
22 M. G. B. Drew, J. Nelson, F. Esho, V. McKee and S. M. Nelson, *J. Chem. Soc., Dalton Trans.*, 1982, 1837.
23 P. Dapporto, G. De Munno, A. Sega and C. Mealli, *Inorg. Chim. Acta*, 1984, **83**, 171.
24 O. Horner, J.-J. Girerd, C. Philouze and L. Tchertanov, *Inorg. Chim. Acta*, 1999, **290**, 139.
25 P. Gili, M. G. Martín Reyes, P. Martín Zarza, M. F. C. Guedes da Silva, Y. Y. Tong and A. J. L. Pombeiro, *Inorg. Chim. Acta*, 1997, **255**, 279.
26 N. G. Connelly and W. E. Geiger, *Chem. Rev.*, 1996, **96**, 877.
27 D. G. Lonnon, G. E. Ball, I. Taylor, D. C. Craig and S. B. Colbran, *Inorg. Chem.*, 2009, **48**, 4863.
28 A. B. P. Lever, *Inorganic Electronic Spectroscopy*, Elsevier, 1984.
29 R. Blessing, *Acta Crystallogr., Sect. A: Fundam. Crystallogr.*, 1995, **51**, 33.
30 A. Altomare, G. Cascarano, C. Giacovazzo and A. Guagliardi, *J. Appl. Crystallogr.*, 1993, **26**, 343.
31 G. M. Sheldrick, *SHELXL-97*, University of Göttingen, Germany, 1997.
32 L. Farrugia, *J. Appl. Crystallogr.*, 1997, **30**, 565.
33 S. Alvarez, P. Alemany, D. Casanova, J. Cirera, M. Llunell and D. Avnir, *Coord. Chem. Rev.*, 2005, **249**, 1693.
34 S. M. Baldeau, C. H. Slinn, B. Krebs and A. Rompel, *Inorg. Chim. Acta*, 2004, **357**, 3295.
35 A. Wada, S. Ogo, S. Nagatomo, T. Kitagawa, Y. Watanabe, K. Jitsukawa and H. Masuda, *Inorg. Chem.*, 2002, **41**, 616.
36 C. Duboc, T. Phoeung, D. Jouvenot, A. G. Blackman, L. F. McClintock, J. Pécaut, M.-N. Collomb and A. Deronzier, *Polyhedron*, 2007, **26**, 5243.
37 R. Hoffmann, B. F. Beier, E. L. Muetterties and A. R. Rossi, *Inorg. Chem.*, 1977, **16**, 511.